

# THE DESIGN AND APPLICATION OF A SQUEEZE FILM DAMPER BEARING TO A FLEXIBLE STEAM TURBINE ROTOR

by

**Malcolm E. Leader**

**Turbomachinery Consultant  
Applied Machinery Dynamics Company  
Dickinson, Texas**

**John K. Whalen**

**Vice President and Engineering Manager  
Turbo Components and Engineering  
Houston, Texas**

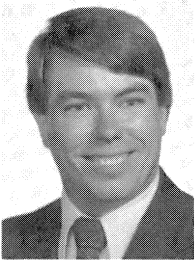
**Godfrey G. Grey**

**Principal Rotating Equipment Engineer  
ARCO Chemical Co.  
Channelview, Texas**

and

**Thomas D. Hess, Jr.**

**Machinery Advisor  
ARCO Chemical Co.  
Newtown Square, Pennsylvania**



*Malcolm E. Leader is a Turbomachinery Consultant and Owner of Applied Machinery Dynamics, in Dickinson, Texas. He is currently involved in the design, testing, modification, and installation of rotating equipment. He spends time doing theoretical design audits and working in the field implementing changes and overseeing installations.*

*Mr. Leader obtained his B.S. and M.S. degrees from the University of Virginia (1977, 1978). While there, he worked extensively on experimental rotordynamics and hydrodynamic bearing design. Mr. Leader has written several papers on the subjects of experimental rotordynamics, bearing design, design audits for rotating equipment, and practical implementation of rotordynamic programs.*

*Mr. Leader is a member of ASME, Sigma Xi, and the Houston Chapter of The Vibration Institute. He is a registered Professional Engineer in the State of Texas.*



*John K. Whalen is the Engineering Manager and Vice President of TCE. Mr. Whalen received his B.S.M.E. degree from the Rochester Institute of Technology (1981). He spent seven years at Turbodyne Steam Turbines (Dresser-Rand) in Wellsville, New York, as a Product Engineer in the Large Turbine Engineering Department and as an Analytical Engineer in the Rotordynamics Group of the Advanced Engineering and Development Department.*

*In January 1988, Mr. Whalen accepted a position with Centritech, as the Assistant Chief Engineer. In April 1989, he was promoted to*

*Manager of Engineering. In January 1991, he left Centritech to help start TCE. At TCE, Mr. Whalen is responsible for the Engineering Department and Engineering for the product lines, which include babbitted journal and thrust bearings, labyrinth seals, and related engineering services.*

*Mr. Whalen is a member of ASME, STLE, and The Vibration Institute. He is a registered Professional Engineer in the State of Texas.*



*Godfrey G. Grey is a Principal Rotating Equipment Engineer at ARCO Chemical Co. His responsibilities, since joining ARCO in 1991, are identifying rotating and reciprocating machinery problems, analyzing the root causes, and recommending changes to design, maintenance, and operation. In addition, he supervises the major equipment overhauls and the Predictive Maintenance Programs. Prior to joining ARCO, Mr. Grey worked for Shell Chemical for more than 11 years as a Rotating Equipment Engineer with similar responsibilities.*

*Mr. Grey has a B.S. degree (Mechanical Engineering) from The City College, The City University of New York (1975). He is an active member of The Vibration Institute and a Registered Professional Engineer in the State of Texas.*

## ABSTRACT

A critical multistage steam turbine in a large chemical plant experienced high vibration levels and frequent repairs. Numerous failures occurred while passing through the rotor's first critical speed including heavy rubs. An analysis of the rotor/

bearing system dynamics revealed that the rotor was highly sensitive to unbalance. Several different solutions were modelled and evaluated. Modifications to the shaft were rejected and modifications to the machine case were too costly and too time consuming. A combination tilting pad journal bearing encased in a squeeze film damper was proposed along with the addition of two nonfunctional "dummy" wheels that lowered the first critical speed, improving the separation margin. The damper is supplied with normal oil pressure that then feeds the journal bearing. This solution was implemented, resulting in a significant reduction in rotor amplification factor from 14.8 to 4.2 and greatly reduced vibration amplitudes throughout the operating speed range eliminating the rotor rubs. This machine is now operating well and has survived many startups and shutdowns without incident.

## INTRODUCTION

The steam turbine is used to drive a critical service cooling water pump. Two additional electric motor-driven pumps comprise the rest of the cooling water system. All three pumps are usually kept in continuous operation with the turbine driven pump used for emergency cooling water in case of a plant electric power failure.

This cooling water pump system has been in service for 20 years. The original operating mode was for the two electric motor driven pumps to operate continuously with the steam turbine driven pump maintained in standby (auto start) mode in the event of a power failure. Later additions to the plant increased the cooling water demand resulting in the need to run all three pumps continuously.

The original steam turbine supplied with the cooling water system was a single stage emergency service design. When continuous service became necessary, large steam consumption and poor efficiency dictated the purchase of a new multistage turbine in 1989. At the time of purchase, no lateral or torsional rotordynamics analyses were requested or performed on the new steam turbine system.

The cooling water machine train is outlined in Figure 1. It consists of a steam turbine driving through a parallel shaft gearbox and a right angle gearbox to a large (85,000 gal/min) vertical centrifugal pump. The turbine speed of 3,600 rpm is reduced to a pump speed of 440 rpm by the speed reducers. The turbine and parallel shaft gear are connected through a disc pack coupling with a short spacer. The parallel shaft and right angle

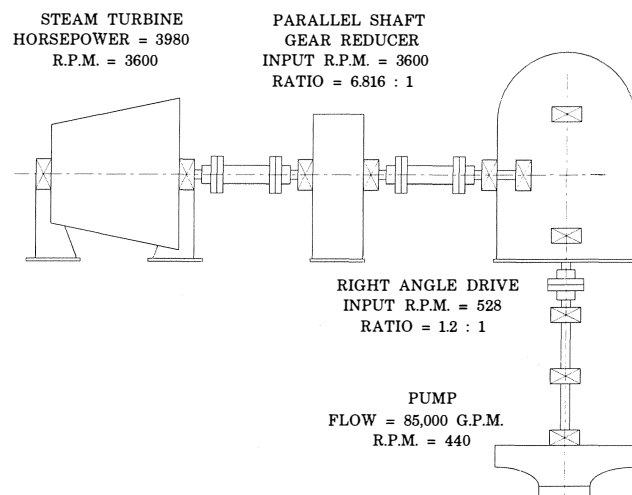


Figure 1. Schematic of Cooling Water Pump Train Layout.

gears are connected with a grease lubricated gear coupling. The right angle gear and the pump are rigidly coupled. A photograph of the steam turbine installation is shown in Figure 2.

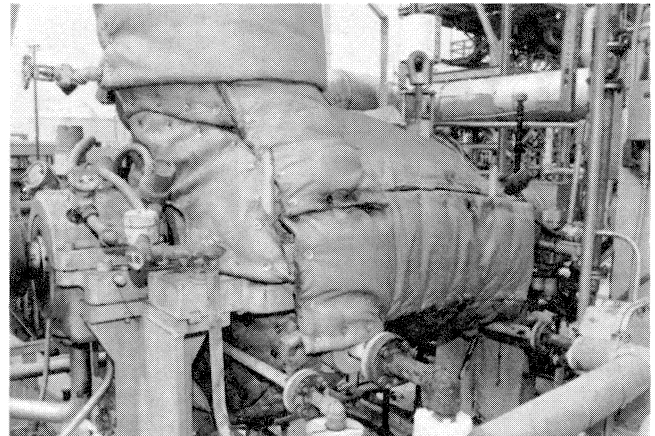


Figure 2. Photograph of Steam Turbine Installation.

## OPERATING HISTORY

Vibration problems were encountered shortly after the initial startup in 1989. The shaft displacement vibration levels encountered while passing through the critical speed range around 3,000 rpm were more than 4.0 mil and full speed vibration levels were 2.0 to 3.0 mil. However, the turbine was kept in operation at this time. The turbine received a major overhaul during a scheduled plant shutdown in 1991 to determine the cause of the high vibration. A severely bowed shaft (about 7.0 mil) was found at this time and a new shaft was manufactured. The rotor was reassembled and shop balanced to 4W/N or less than 1.2 oz-in.

The turbine was reinstalled and started with vibration levels as high as before along with a seal steam leak. The poor operation was blamed on a faulty repair and the turbine was sent to another repair shop. The rotor was again found to be bowed and again a new shaft was manufactured. The stacked rotor was very carefully balanced to the limit of the balancing machine, well below 4W/N.

The cause of the bowed rotors was thought to be "operator error" as the tendency of the operators was to stop the acceleration of the turbine during startup when the vibration became severe. Unfortunately, this usually occurred in the middle of the critical speed range. Pausing at the critical speed caused vibrations to increase further resulting in permanent rotor damage. Several subsequent attempts at restarting after the initial rubs only increased the damage to the rotor.

Although this turbine was equipped with a programmable governor, this feature was not in use and the normal procedure was to bring the turbine up to minimum governor speed manually on the trip and throttle valve. The speed was then set with the electronic governor speed adjust buttons. After the second repair in 1990, the governor was programmed to slow roll the turbine and then automatically accelerated to minimum governor speed with the operator having to only push two buttons. As with all changes, this change was accepted by some while other operators continued to adjust the turbine speed manually.

At this point, the first attempt at using the installed eddy current probes and monitors (instead of seismic data) was performed. The next startup was observed with instrumentation and the apparent cause of the high vibration was a radial rub. This seemed to correlate with the observed operating symptoms and the bowed rotor damage. The rub occurred at a speed well below

the published critical speed. The presence of the rub was diagnosed from the flat orbit shape and phase angle changes. Significant changes in the slow roll vectors were seen from run to run and at different times. Slow rolling the rotor seemed to "roll-out" the rub induced bow.

The turbine mounting was examined to ensure that the steam casing was free to expand evenly without distortion when heated, as this was thought to be a possible cause for the rub. All shipping bolts and slides were found to be free and well lubricated. The thermal growth was observed during startup and found to be normal.

Several startups were attempted to "rub-out" whatever was impinging on the shaft. During each startup, at an arbitrary value of 2.0 mil peak-to-peak at the displacement probes, the turbine was shut down and put on slow roll until the low speed displacement vectors returned to near their initial values. This "rubbing out" process appeared to be working because the speed at which the 2.0 mil limit was reached increased with each startup until the speed reached the lower end of the critical speed range (2400 rpm). After this, there was no gain due to the critical speed response which increased amplitudes rapidly. The pump was urgently needed in service so a governor controlled startup was attempted. More than 3.0 mil were observed passing through the critical speed and full speed was achieved with shaft amplitudes less than 1.0 mil. This was considered acceptable and the pump was left in service.

A recommendation was made at this time to perform a lateral and torsional analysis of the machine train, because no analysis had been performed when the replacement turbine was purchased in 1989. Startup and operation continued to be problematic until a plant turnaround in the Fall of 1994 when another complete overhaul was done. The next startup saw more than 75 mil of case motion recorded by a brave soul with hand held equipment. Upon opening the machine, extensive damage to the turbine was found. The shaft was bowed beyond repair and at this point a complete rotordynamics analysis was commissioned.

## ROTORDYNAMICS ANALYSIS

The initial evaluation of a rotor bearing system consists of detailed measurements of the components. In this case, no previous model of the rotor was available. The rotor is measured, disks and other components are weighed, and polar and transverse moments of inertia are calculated. The bearings are examined and measured including critical clearances and seal dimensions. Finally the casing is evaluated for mass and stiffness properties and to see if any beneficial casing modifications are possible. These are critical steps that must be carefully completed. An error at the modelling stage will not be detectable later in the analysis.

At this point several "rules-of-thumb" can be employed to size up the project. First, the bearing span,  $L_s$ , to shaft diameter,  $D_s$ , ratio is evaluated. Usually an  $L_s/D_s$  ratio greater than 10 will indicate a rotor with a high amplification factor. In this case, the main shaft diameter is 6.0 in and the bearing span is  $73\frac{1}{4}$  in for a ratio of 12.2, which indicates a very flexible shaft. The shaft stiffness is approximated by beam theory at 233,000 lb/in. For a well-behaved machine, the combined bearing stiffnesses should be less than twice the shaft stiffness. One initial consideration was to increase the shaft diameter. This would increase the shaft stiffness but that would also increase the critical speed closer to operating speed so that modification idea was abandoned.

The existing bearings were five pad tilting pad bearings. First they were evaluated for their static loading. The governor end bearing is 4.0 in in diameter and 3.0 in in long and carries 464 lb. The static unit loading is defined as  $W/L_s D_s$  or 38.7 psi for this end. The exhaust end bearing is 5.0 in in diameter and 3.75 in

long and carries 645 lb for a unit loading of 34.4 psi. These are low specific loads and the lower the specific load, the "softer" the hydrodynamic film. Increasing the bearing diameter or axial length is one way of reducing the bearing stiffness however, increasing the bearing L/D ratio above 0.75 yields diminishing benefits. In this case, the existing bearings were about as good as possible for a conventional design in the space allowed.

The stiffness and damping coefficients for the existing bearings were calculated and the results are shown in Figures 3 and 4. The horizontal and vertical values are nearly equal with the exhaust end greater than the governor end. At operating speed (3,600 rpm) the stiffnesses range from 450,000 to 750,000 lb/in and the damping values range from 1,750 to 2,250 lb-sec/in.

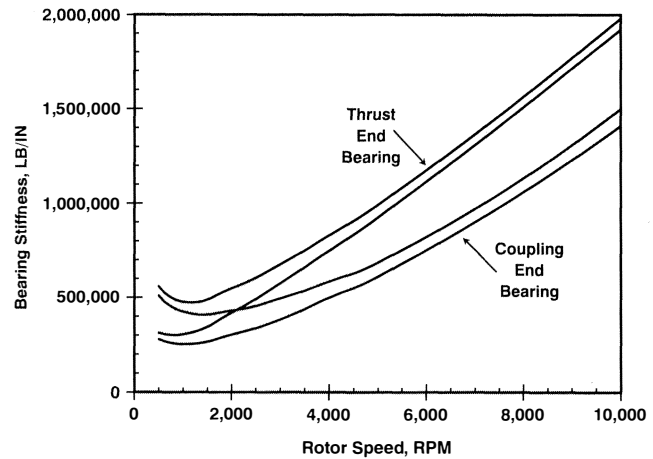


Figure 3. Principal Stiffness Coefficients of Original Five-Pad Tilting Pad Journal Bearings.

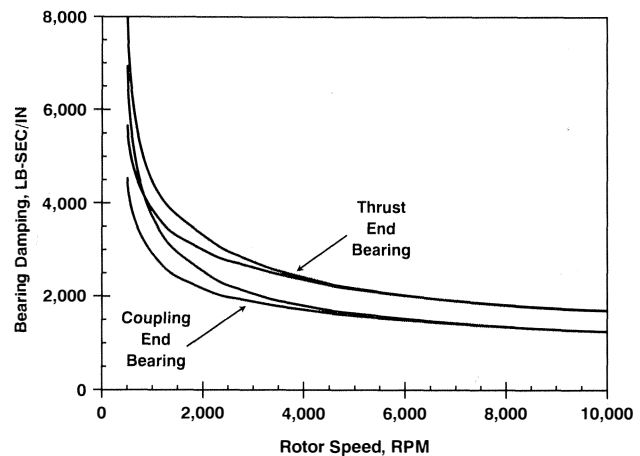


Figure 4. Principal Damping Coefficients of Original Five-Pad Tilting Pad Journal Bearings.

The computer generated rotor model, Figure 5, shows that there is one compound Curtis (impulse) stage and six Rateau (pressure) stages. This model is used to generate an undamped critical speed map, Figure 6, which displays the first three critical speeds as a function of bearing support stiffness. As bearing stiffness increases from 10,000 lb/in to 100,000 lb/in, the first critical speed frequency increases rapidly until the bearing stiffness reaches about 500,000 lb/in. Then the critical speed frequency increases more slowly until, at 1,000,000 lb/in,

it becomes asymptotic and increasing the stiffness further will not raise the critical speed. Cross plotted on this chart are dynamic stiffness coefficients. These are a frequency dependent summation of the stiffness and damping coefficients:

$$K_{dx} = \sqrt{(K_{xx})^2 + (\omega C_{xx})^2}$$

and

$$K_{dy} = \sqrt{(K_{yy})^2 + (\omega C_{yy})^2}$$

$$\text{where } \omega = \frac{2\pi \text{ RPM}}{60} \quad \frac{\text{RAD}}{\text{SEC}}$$

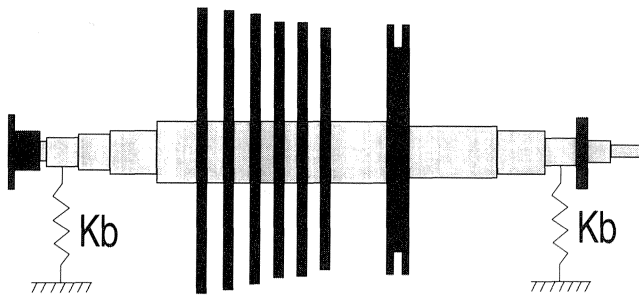


Figure 5. Computer Model of Original Unmodified Steam Turbine Rotor.

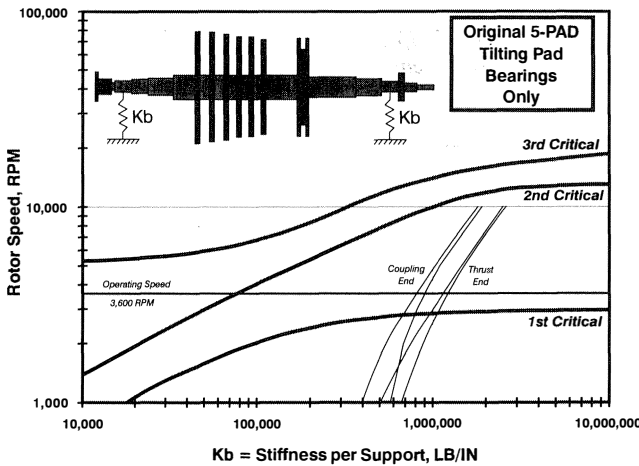


Figure 6. Undamped Critical Speed Map for Unmodified Steam Turbine Rotor with Dynamic Stiffness Coefficients.

Here the damping coefficients are multiplied by frequency to account for their behavior as a dynamic stiffness. These dynamic coefficients more accurately predict the critical speeds on the undamped critical speed map. The ratio of combined dynamic bearing stiffness to shaft stiffness is about 8.5 to one that means these bearings are too stiff to assure a well-damped unbalance response. The undamped critical speed mode shape with the original bearings in Figure 7 helps explain the difficulty in controlling this rotor's vibrations with conventional bearings. This shaft is so flexible that node points appear next to the bearings and the probe areas. This situation has two consequences. The effective bearing damping is reduced by restricting motion in the hydrodynamic film and having the proximity probes close to the nodes makes them indicate a low percentage

of actual shaft center motion at the critical speed. Unfortunately no actual records of amplitude and phase angle versus speed exists for the original rotor bearing system. The machine wrecks and high amplitude observations were enough to guide the plant in extreme caution during startup and operation.

This machine is designed to accommodate two additional wheels for other horsepower situations. Taking advantage of these blank spaces on the rotor, the final design included adding two "dummy" disks at the locations normally occupied by the other Rateau stages. The reason for adding mass to the rotor is to lower the critical speed, increasing the separation margin between it and the operating speed. The rotor model with the dummy wheels is shown in Figure 8.

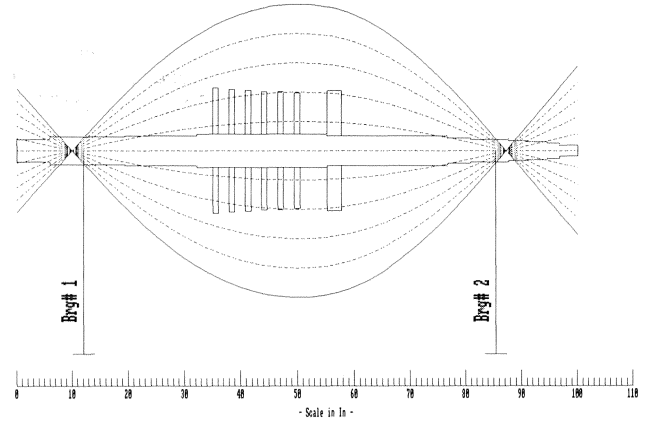


Figure 7. Critical Speed Mode Shape for Original Rotor and Five-Pad Tilting Pad Bearings.

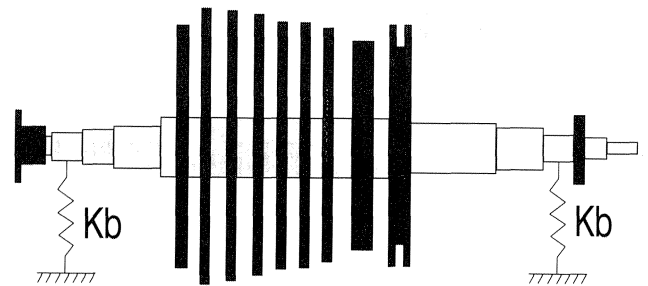


Figure 8. Computer Model of Steam Turbine Rotor Modified with "Dummy" Disks.

Using the actual stiffness and damping coefficients and the rotor model, the predicted rotor amplitude response to 4W/N (1.2 oz-in) imbalance placed at the rotor center is plotted in Figure 9 for the thrust end probe location and the rotor center. Note that the probe detects only about 27 percent of the center span amplitude. The predicted amplification factor is 14.8 with the maximum response at 3,030 rpm. This predicted response agrees with the observed turbine vibration patterns.

To increase the accuracy of the unbalance response modeling, a support substructure was included in the computer program. Ideally, impact testing or finite element modeling would have been performed to get stiffness and mass properties from the machine casing. This project went from analysis to startup in 10 days, so known values from similar machines were used. The authors chose 3,000,000 lb/in horizontal support stiffness and 5,000,000 lb/in vertical support stiffness. Ten percent of critical damping was also included in the structural model.

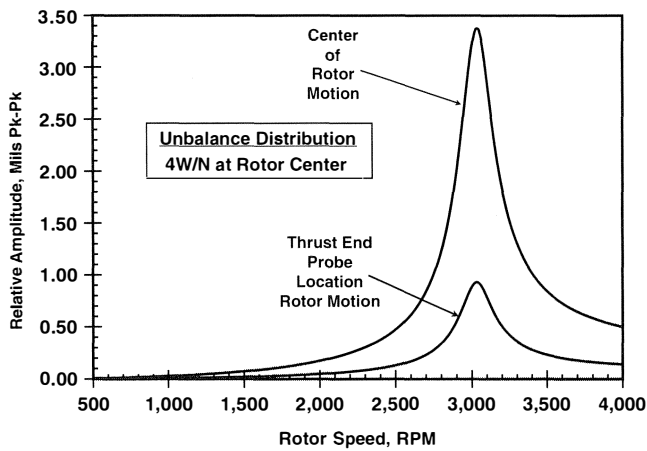


Figure 9. Predicted Unbalance Response for Original Rotor and Bearings.

### SQUEEZE FILM DAMPER THEORY

The underlying idea behind the squeeze film damper is to optimize the available damping to dissipate rotor vibration energy. Because a large damping value is also a dynamic stiffness, it is vital to first reduce the bearing stiffness and then optimize the damping. Just adding damping to a rotor system with stiff bearings is doomed to failure. Allowing freedom of movement by reducing bearing stiffness allows the damping in the oil film to remove vibrational energy as heat and reduce rotor displacement amplitudes. This concept is excellent when applied to rotor bearing systems that meet certain criteria but nearly useless in other situations. The prime candidate is a very flexible rotor operating above its first critical speed. Squeeze film dampers are commonly applied to jet engine shafts mounted in rolling element bearings that are very stiff and have little damping. They are also employed to solve unstable subsynchronous vibration problems. Large heavy rotors are not good applications because of the difficulty in centering the damping film. Geared systems that have large changes in gear tangential and separation forces as load changes are also not suitable because of the large change in bearing (and seal) eccentricity that can occur.

A squeeze film damper is defined as a journal bearing where there is no rotation but translational motion is allowed. In this case, the tilting pad bearing is enclosed by an outer shell with an annular clearance. The oil in the cavity is retained by O-rings that also serve to center the journal in the damper housing. A diagram of this arrangement is shown in Figure 10. The mathematical theory for this design is primarily based on the work of Gunter, Barrett, and Allaire [1]. There are numerous papers and articles describing both squeeze film damper theory and experimental testing. Nikolajsen and Holmes [2] analyzed a flexible rotor and the control of synchronous vibrations by damper isolation. Childs [3] presents a detailed discussion of the mathematics of squeeze film dampers and a good discussion about the practical application of dampers. The limitations are also discussed including the discrepancies between theory and measurements. Vance [4] has a thorough analysis of the squeeze film damper including nonlinear effects. One nonlinear phenomena is a "jump" effect where a sudden change in rotor response occurs when large synchronous amplitudes are encountered. Zeidan and Vance [5] examine the effects of cavitation and the entrainment of air in the damper film. If there is no cavitation in the damper film, a  $2\pi$  film is developed and a full circumferential dynamic pressure wave is generated. If cavitation occurs, the

positive pressure region is reduced to a  $\pi$  film or 180 degrees. Much of the work, both experimental and theoretical, is concerned with jet engine dampers applied to rolling element bearings operating at much higher frequencies than the 3,600 rpm machine in this analysis.

End seals are needed to retain the oil film and elastomer O-rings are chosen for the design. A circumferential distribution groove is required because the tilting pad bearing oil is supplied by the oil flowing through the damper. Ideally, translational motion will generate a pressure profile, as shown in Figure 11. Several researchers have reported pressure fluctuations in the supply groove. The inner bearing design chosen was a 4-pad tilting pad bearing with load between pads. The stiffness and damping of this bearing by itself is not much different from the original bearing, but it does have the advantage of having equal horizontal and vertical stiffness and damping characteristics. This justifies the simplification of the damper analysis that limits us to centered circular shaft orbits since everything is symmetrical. The assumption is that the film is cavitated. The stiffness and damping are calculated using a computer program developed by Lloyd E. Barrett at the University of Virginia. The dynamic stiffness and damping coefficients for a cavitated film are calculated from the following equations:

$$K = \frac{2 \mu R L^3 \epsilon \omega}{c^3 (1 - \epsilon^2)^2}$$

and

$$C = \frac{\pi \mu R L^3}{2 c^3 (1 - \epsilon^2)^{3/2}}$$

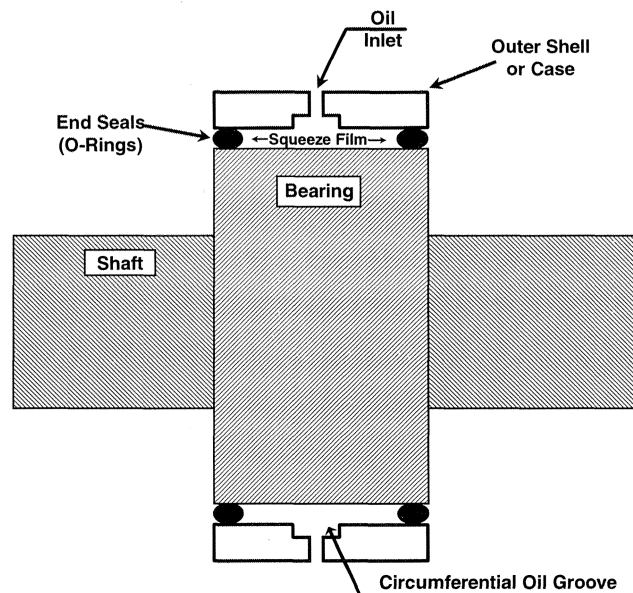


Figure 10. Typical Squeeze Film Damper Construction.

In these equations,  $K$  and  $C$  are the damper stiffness and damping,  $\epsilon$  is the eccentricity ratio,  $\mu$  is the oil viscosity,  $\pi$  is 3.1415926 . . . ,  $R$  is the damper radius,  $L$  is the damper length,  $\omega$  is the frequency in radians per second, and  $c$  is the damper radial clearance. Note that clearance and length are both cube factors and strongly affect the coefficients. Many researchers have found that experimental results do not agree with the coefficients predicted by these simple equations. However, in

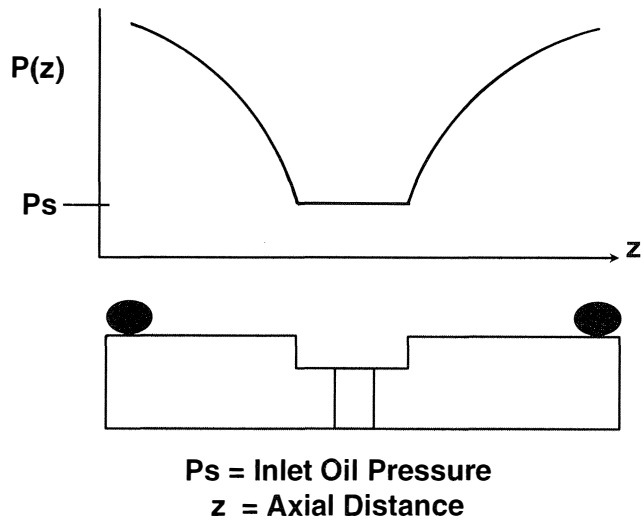


Figure 11. Axial Pressure profile of Typical Squeeze Film Damper.

this case, the predicted combined bearing and damper coefficients were sufficient to solve the problem. Only normal oil pressure (20 to 40 psig) was available from the lubrication system to feed the damper and the bearing pads. Varying the oil pressure within these limits did not affect the damper performance.

**DESIGN AND TESTING**

In order to design a damper that is centered under load, the stiffness of the O-rings must be known. This data is not readily available in the manufacturer's literature so a test fixture was constructed to test the O-rings experimentally. The setup used to conduct these tests is shown in Figure 12. Several O-rings with different compounds and cross section were tested. The final selection was a 90-durometer fluorocarbon (oil resistant) material with a cross section of 0.210 in. Both 6.0 in and 7.75 in diameter rings were tested. One design parameter is the width of the O-ring groove. If this groove is too narrow and fills with the elastomer under load, the stiffness of the O-ring will not be linear. To avoid this, a groove width of 0.281 in was used.

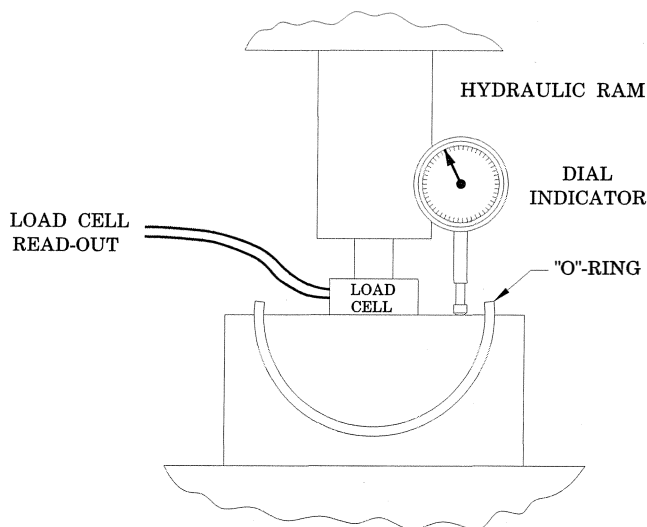


Figure 12. O-Ring Load-Deflection Experimental Test Setup.

Typical results of these tests are shown in Figure 13. The 6.0 in diameter ring setup has a stiffness of 18,000 lb/in and the 7.75 in diameter ring setup has a stiffness of 24,000 lb/in.

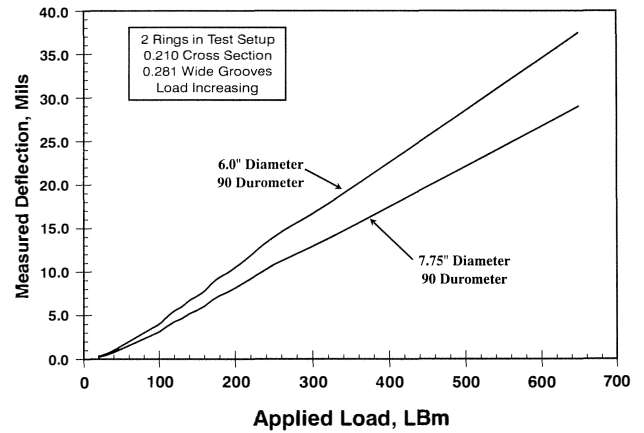


Figure 13. Load-Deflection Test Results to Determine O-Ring Stiffness.

To end up with the inner bearing centered in the damper after the rotor load is applied, the O-ring grooves are cut eccentric with the bearing bore and the rings are preloaded so that the top (unloaded area) of the damper O-ring is still under some compression when the damper is centered. Using the 7.75 in diameter ring as an example, if initial preload of 10 percent is wanted, then this creates an additional load equal to the compression times the O-ring stiffness. This load is:

$$\delta = 0.210 \text{ INCH Diameter} \times 10\% = 0.021 \text{ INCHES}$$

$$K = 24,000 \text{ LB/IN (Measured O-ring Stiffness)}$$

$$K\delta = 504 \text{ LBf}$$

Thus, the total load on the bottom of the O-ring is this preload plus the 650-lb static shaft load from the rotor or 1,154 lb total. Referring to Figure 14, the lower ring compression will be 1,154/24,000 or 0.048 in. To get this initial 10 percent compression on the top O-ring, the top groove depth plus the clearance must equal 90 percent of the O-ring cross section diameter minus the damper clearance. From the optimization procedure, the desired damper radial clearance is 0.010 in so the top O-ring groove depth is 0.9(0.210)-0.010 or 0.179 in. On the bottom half of the damper we need a groove depth of O-ring cross section minus the compression, minus the radial clearance or 0.210-0.048-0.010 or 0.152 in. This means that the eccentricity on the O-ring groove is 0.179-0.152 = 0.027 in. Figure 14 indicates that without the shaft load, the top of the damper has no clearance. With shaft load applied, the damper has an even 10-mil clearance on all sides. The final bearing assembly cutaway is Figure 15 and Figure 16 is a photograph of the actual bearing half with the inner and outer shells, supply groove and bearing inlet orifices.

The calculated stiffness and damping values of the damper alone are not important. What we need are the actual resultant stiffness and damping coefficients. These are calculated with equations developed by Nicholas [6]. These equations for the horizontal direction are:

$$K_{EQXX} = \frac{\hat{K}_{SX} K_{XX} (\hat{K}_{SX} + K_{XX}) + \omega^2 (K_{XX} C_{SX}^2 + \hat{K}_{SX} C_{XX}^2)}{(\hat{K}_{SX} + K_{XX})^2 + \omega^2 (C_{SX} + C_{XX})^2}$$

and

$$C_{EQXX} = \frac{K_{XX}^2 C_{SX} + (\hat{K}_{SX}^2 C_{XX} + \omega^2 C_{SX} C_{XX} (C_{SX} + C_{XX}))}{(\hat{K}_{SX} + K_{XX})^2 + \omega^2 (C_{SX} + C_{XX})^2}$$

Where:

$$\hat{K}_{SX} = K_{SX} - m_{SX} \omega^2 \quad m_{SX} = \text{Support Mass}$$

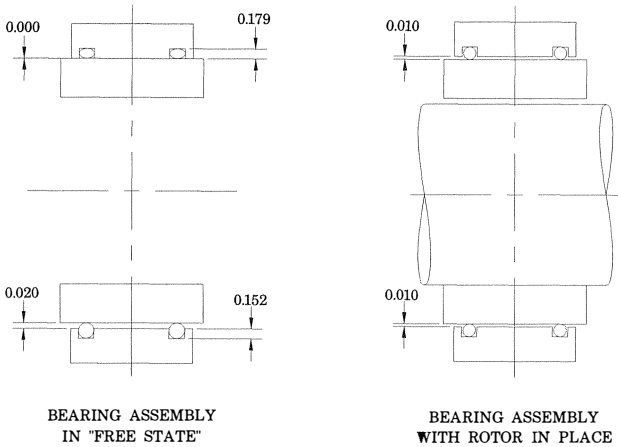


Figure 14. Damper Construction Details Showing Eccentric Setup to Center Assembly under Load.

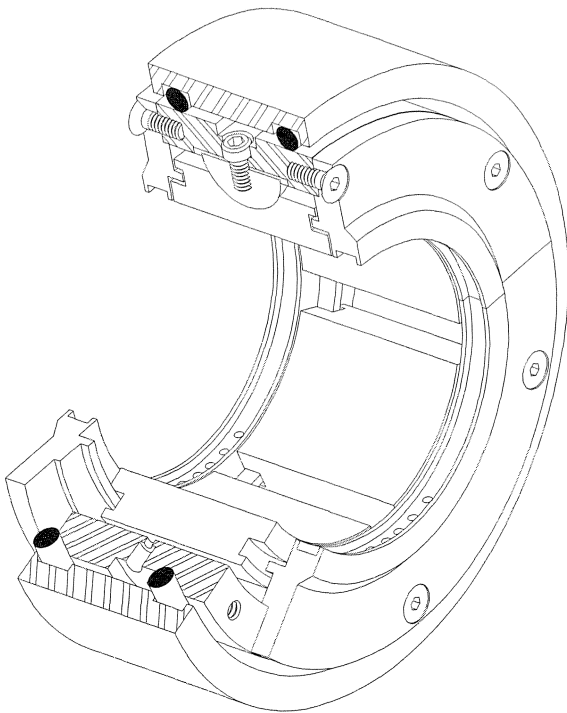


Figure 15. Isometric View of Complete Four-Pad Tilting Pad and Squeeze Film Damper Bearing.

Here,  $\omega$  is the frequency in radians per second and the SX subscript is the damper characteristic while the subscript XX is

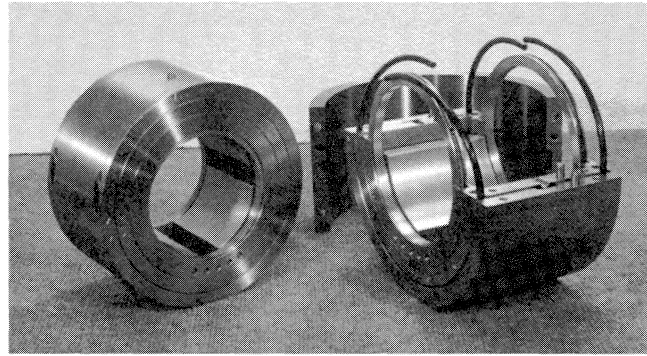


Figure 16. Photograph of Actual Squeeze Film Damper at Splitline.

the tilting pad bearing characteristic. In Figures 17 and 18, the effective stiffness and damping values of the combined system are seen for the governor end bearing. The final exhaust end bearing coefficients are similar. It is important to note that the damping values *have not increased* and in fact are about one-half of the calculated damping from the rigidly mounted tilting pad bearing alone. The big change is the drop in effective stiffness to near 200,000 lb/in for each bearing. This stiffness decrease is the key to the success of this design. The undamped rotor first critical speed mode shape (Figure 19) confirms that now the bearings are not near node points but have enough relative amplitude to make the bearing damping effective.

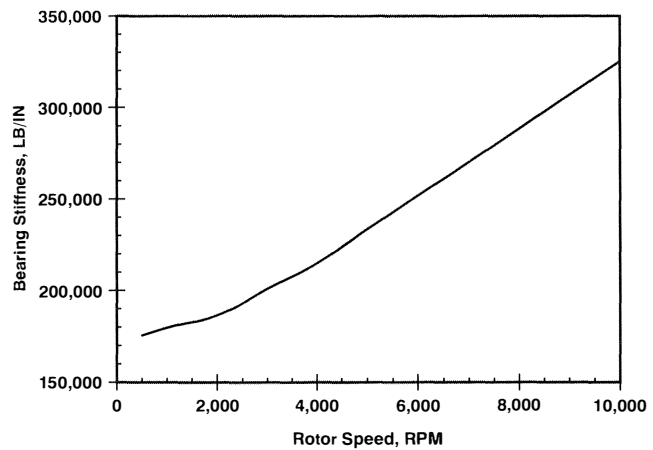


Figure 17. Combined Stiffness of Four-Pad Tilting Pad Bearing and Squeeze Film Damper Assembly.

Now, when the thrust end probe amplitude is compared with the center span amplitude (Figure 20) the probe "sees" 39 percent of the maximum rotor amplitude. The calculated unbalance response for the original bearings is compared in Figure 21, with the actual damper bearing that was manufactured and installed. With the same applied imbalance, the center span amplitude has been reduced from 3.4 mil to 1.0 mil and the frequency has dropped from 3,030 rpm to 2,610 rpm. The change in critical speed frequency is due to both the decrease in bearing stiffness and the addition of the extra mass from the dummy wheels. At the exhaust end probe location, Figure 22, the critical speed amplitude drops from 0.93 mil to 0.36 mil. For both locations, the amplification factor decreased from an intolerable 14.8 to a controllable 4.2.

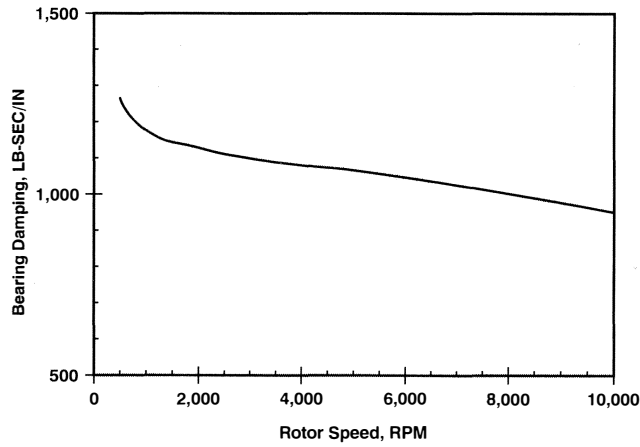


Figure 18. Combined Damping of Four-Pad Tilting Pad Bearing and Squeeze Film Damper Assembly.

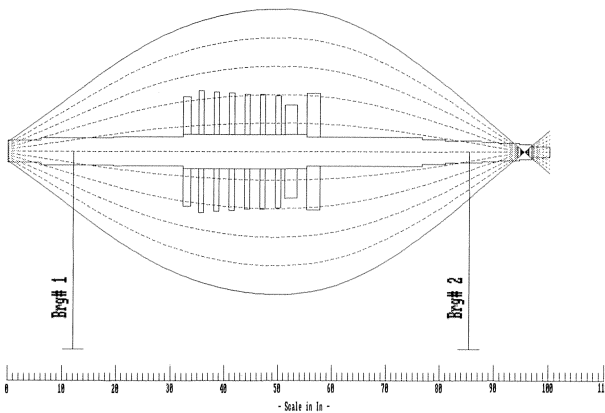


Figure 19. Critical Speed Rotor Mode Shape with “Dummy” Disks and Squeeze Film Damper Bearings.

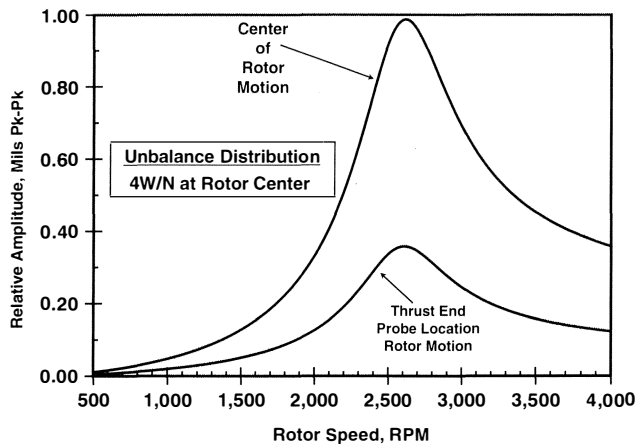


Figure 20. Predicted Unbalance Response at Rotor Center and Thrust End Probe Location with Modified Rotor and Four-Pad Bearings with Squeeze Film Damper.

The final proof of the design is the actual field test. The actual amplitude and phase are shown in Figure 23 from the thrust end horizontal displacement probe captured during a startup after the damper bearing was installed. The peak amplitude occurs at

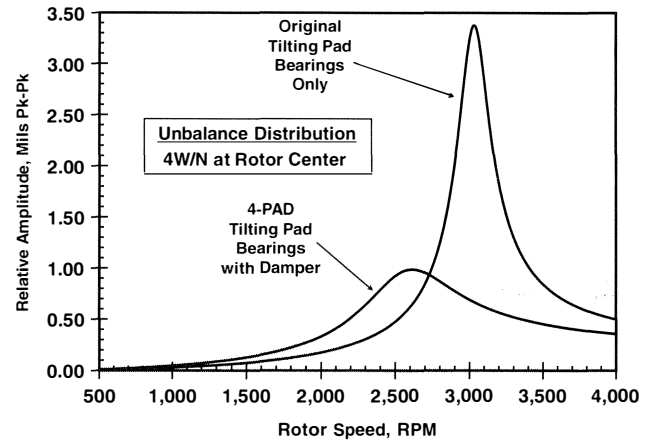


Figure 21. Comparison of Center Span Amplitude—Original Bearings vs Squeeze Film Damper Bearings.

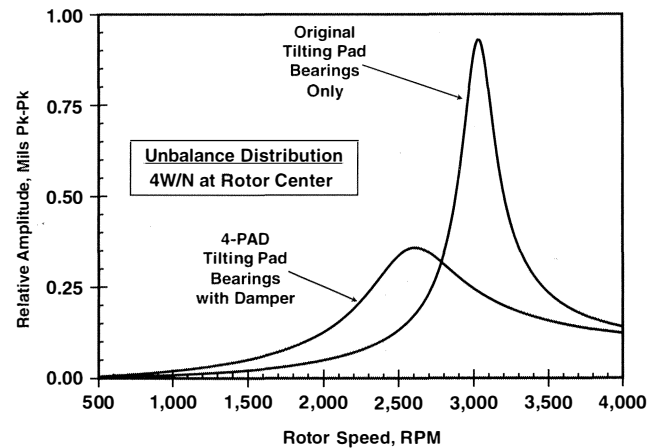


Figure 22. Comparison of Exhaust End Amplitude—Original Bearings vs Squeeze Film Damper Bearings.

2625 rpm with a maximum reading of 1.34 mil and an amplification factor of 4.2. This matches the predicted response very closely except in maximum amplitude. The predicted vs actual synchronous amplitude vs speed plots are compared in Figure 24 for added clarity. There was some wet steam present during this startup which may have increased the overall amplitude of the field measurements.

Only shaft motion relative to the case was measured. Casing velocity was reported to be less than 0.08 in/sec peak at any point. The synchronous shaft displacement orbits were almost completely circular and the shaft centerline position measurements (DC gap voltage) showed the shaft move directly straight up from rest to full speed. These facts further justify the simplified assumptions made in the initial damper design stage. It would have been insightful to have recorded the relative motion of the bearing inside the damper, but this is a production machine and is not readily available for experimentation.

### CONCLUSIONS

A critical turbomachine must perform reliably even under less than ideal operating conditions. The turbine described in this paper was not able to do this because of extreme sensitivity to unbalance forces. Space and time limitations eliminated altering the turbine case and increasing the shaft diameter would have caused an operating speed interference with the critical speed.



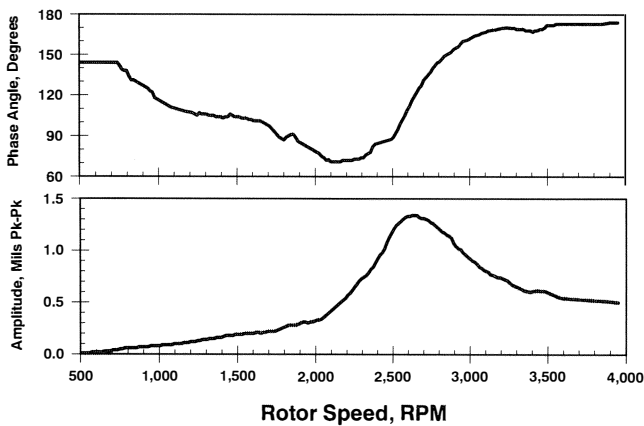


Figure 23. Measured Amplitude and Phase Angle from Thrust End Horizontal Displacement Probe during a Turbine Solo Run.

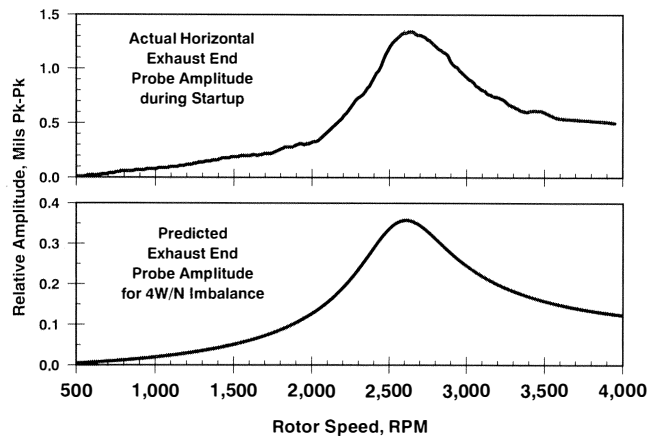


Figure 24. Predicted Thrust End Unbalance Response Compared to Actual Synchronous Vibration.

The bearings were modified by adding a squeeze film damper in series with the tilting pad bearing. A simplified damper analysis was used. This combination lowered the bearing stiffness and damping values. The lower stiffness allowed rotor motion at the bearings making the available damping much more effective. In addition, two "dummy" wheels were mounted on the shaft to lower the critical speed frequency further. The effect was to lower the critical speed amplification factor from 14.8 to 4.2 and reduce overall amplitudes. This machine now runs through its

critical speed without rubs and operates continuously with displacement probe amplitudes from 0.4 to 0.6 mil peak-to-peak.

#### REFERENCES

1. Gunter, E. J., Jr., Barrett, L. E., and Allaire, P. E., "Design and Application of Squeeze Film Dampers for Turbomachinery Stabilization," *Proceedings of the Fourth Turbomachinery Symposium*, The Turbomachinery Laboratory, Texas A&M University, College Station, Texas (1975).
2. Nikolajsen, J. L. and Holmes, R., "Investigation of Squeeze-film Isolators for the Vibration Control of a Flexible Rotor" *Jnl. Mech. Eng. Sci.*, 21 (4), pp. 247-252 (1979).
3. Childs, D. W., *Turbomachinery Rotordynamics*, New York, New York: John Wiley & Sons, (1993).
4. Vance, J. M., *Rotordynamics of Turbomachinery*, New York, New York: John Wiley & Sons, 1988.
5. Zeidan, F. Y. and Vance, J. M., "Cavitation Effects on the Pressure Distribution of a Squeeze Film Damper Bearing," *Proceedings of the Texas A&M Workshop on Rotordynamic Instability Problems in High-Performance Turbomachinery*, NASA Conference Publication 3026, pp. 111-132 (1988).
6. Nicholas, J. C., Whalen, J. K., and Franklin, S. D., "Improving Critical Speed Calculations Using Flexible Bearing Support FRF Compliance Data," *Proceedings of the Fifteenth Turbomachinery Symposium*, The Turbomachinery Laboratory, Texas A&M University, College Station, Texas (1986).

#### ACKNOWLEDGMENTS

The authors would like to thank numerous people and organizations for their help and high quality work in completing this project and the preparation of this paper. We thank Revak Turbomachinery for their assistance in gathering all the necessary information on the rotor, bearings and case and for their excellent manufacturing and rebuild work on this turbine. Gary Powers of Power Dynamics Engineering and James Woodruff with ARCO Chemical Co. helped with gathering the field data and startup procedures. John Nicholas and Ed Gunter were invaluable in their assistance and guidance throughout the project. Ken Banks supplied numerous Figures and artwork. Everyone at Turbo Components and Engineering worked tirelessly throughout the 10-day project including helping the authors with the design, testing manufacturing, and final assembly. We also thank Richard Williams, principal reliability engineer with ARCO Chemicals for authorizing the project and believing in the design.

